

RESEARCH ARTICLE

Determination of Different Types of Controller Parameters Using Metaheuristic Optimization Algorithms for Buck Converter Systems

EVREN ISEN 

Faculty of Electrical Engineering, Engineering and Natural Sciences, Bandirma Onyedi Eylul University, Bandirma, 10200 Balikesir, Turkey

e-mail: eisen@bandirma.edu.tr

ABSTRACT The steady-state operation with low error and the fast dynamic response in transient of the DC-DC converter circuits depend on the controller design. The performance of the controller used in DC-DC converters, which vary the level of DC voltage depends on the controller coefficients. Although classical methods are often used to determine these coefficients in controller design, various modern optimization methods have been recently used. In this study, the DC-DC buck converter control simulation is performed with FOPID, PID and TID controllers. Aquila Optimizer, African Vultures Optimization Algorithm and Hunger Games Search optimization algorithms are used to determine the coefficients of these controllers in the literature. However, Fitness-Distance Balance Based Runge Kutta is employed first time for PID controller in buck converter in this study. The performance indices integral absolute error, integral square error, integral time absolute error, and integral time squared error are employed to assess the outcomes. When the results obtained are examined, the FOPID controller gives the best results in the control of the buck converter. These results are obtained by using the coefficients determined by the Fitness-Distance Balance Based Runge Kutta (FDBRUN) optimization algorithm. It has better performance than the other algorithms.

INDEX TERMS Fractional-order PID controller, buck converter, optimization techniques.


I. INTRODUCTION

Power electronics converters are used in photovoltaic systems, smart grids, electric vehicles, uninterrupted power supplies, many industrial applications and products. In power electronics converter topologies, which are generally controlled by pulse width modulation semiconductor power switches are used, and they are controlled by different control strategies. Inductors, capacitors and diodes are also used in various placement depending on the topology. The converter has nonlinear behavior due to the presence of semiconductor elements such as diodes and switches. Therefore, linearization is required for modeling this type of converters.

Power electronics converters have different topologies such as DC-DC, AC-DC or DC-AC converters according to the point of use. Switched mode DC-DC converters are

used in many industrial and technological products which work with DC current. Various DC-DC converters such as buck, boost, buck-boost, sepic, cuk, flyback etc. are used in different applications. The buck converter is a basic non-isolated converter type used in applications where the output voltage is lower than the input voltage.

As in many power electronics converters, Proportional-Integral (PI) or Proportional-Integral-Derivative (PID) controllers are commonly used in buck converter control. In addition, fuzzy logic control [1], sliding mode control [2], hysteresis control [3], dead beat control [4] are frequently used control methods. The controlled electrical quantity varies depending on the application in which the converter is used. PID controller is used in buck converter control in various applications such as speed control in motor applications, photovoltaic (PV) panel power control solar in systems, output voltage control in switched power supplies and many applications. This controller ensures that the applied

The associate editor coordinating the review of this manuscript and approving it for publication was Vitor Monteiro .

error signal reaches the zero value in the shortest time with minimum overshoot. The reference signal is obtained with the algorithm using controller, and switching signal is produced by PWM controller using reference signal. By using the output voltage reference and the measured output voltage produced in a buck converter which the output voltage is controlled, an error is obtained and given to the PID controller. The controller generates the modulation signal that reduces this error to zero, and switching signals are obtained with the help of pulse-width-modulation (PWM). In order to eliminate the effect of a disturbing input, which occurs during the operation of the converter the controller must respond in a robust, dynamic, fast, and stable manner. The dynamic response speed, steady-state response, and stability of the converter depend on the PID coefficients. The determination of these coefficients plays an essential role in the controller performance. There are various methods which are used to determine the coefficients.

The methods used for PID controller coefficient detection can be divided into 3 basic categories: rule-based, formula-based, and optimization-based [5]. In rule-based methods, a rule-based PID-like fuzzy controller was used in motor torque control by using a PD-like fuzzy controller and a parallel PI controller. The use of a minimum rule-based fuzzy controller reduced the challenges experienced in torque control [6]. The Antlion Optimization (ALO) method was used to compare the performance of the fractional-order Particle Swarm Optimization (PSO)-based PID controller with the PSO-based PID controller in the fuzzy-based fractional-order PID controller design utilized in buck converter control. The designed controller has been proved to be more robust under various operating situations such as noise and load variations [7]. Temperature and level control were carried out with real-time experimental application using the fuzzy-rule based automatic adjustment approach in the design of the Internal Model Control (IMC) based PID controller, where only the closed loop time constant parameter needed to be adjusted [8].

The Ziegler Nichols approach, one of the formula-based methods extensively used in PID design, and the Cohen-Coon [9] method were utilized in the design of the PID controller used in the drinking water filtering system, and their performances were compared [10]. For fractional-order PID (FOPID), a novel Ziegler Nichols autotuning approach with smaller overshoot, improved durability and steady-state response, and shorter sitting time was developed [11].

Maximum power point tracking in solar systems was accomplished using a PID controller optimized with the Cuckoo Search Algorithm (CSA). The global maximum power point in the shaded condition was calculated, and the oscillation created at that point is removed [12]. The PSO technique was used to compute the PID controller coefficients of a bidirectional buck-boost converter utilized in small satellite applications. [13]. Moth-Flame Optimization (MFO) was used in wind turbine blade angle control to prevent oscillation in output voltage and power [14]. FOPID controller of a boost

converter was optimized with Queen Bee assisted Genetic Algorithm (QBGA) in [15] to demonstrate the robustness of the proposed controller. In the brushless DC motor control (BLDCM), a new technique called GEO-RPFNN, which the combination of Golden Eagle Optimization (GEO) and Radial Basis Function Neural Network (RBFNN) was proposed. The parameters of the PID controller were optimized with the proposed algorithm, and better results with regarding to torque ripple, power factor and THD of stator current [16]. The coefficients of PID controller were optimized with fuzzy particle swarm optimization algorithm in the buck converter, and the result were given in the integral of time-weighted absolute error (ITAE) performance index [17]. A feedback-type two-degree-of-freedom proportional-integral-derivative (FB2PID) controller was optimized with a bat algorithm (BA) in a parallel dc-dc converter (PDCC). The dynamic response and robustness of the PDCC was improved with the optimization [18]. A four-switch buck-boost dc-dc converter used in Proton Exchange Membrane Fuel Cell (PEMFC) is controlled with FOPID controller for voltage compensation, and the controller parameters were optimized with a stochastic inertia weight PSO algorithm. [19]. Ant colony optimization (ACO) algorithm was used to determine the optimum PID controller parameters of matrix converter [20]. A new designing method based on Strength Pareto Evolutionary Algorithm (SPEA) was proposed for fractional-order PID controller that was used for boost converter control. The better start-up response was achieved with the new method [21]. The PID parameters of zeta converter was optimized with Ant colony Optimization. The zeta converter that is a fourth order system was reduced to second order, and PID coefficients were optimized [22]. LCC resonant converter that was controlled with PID controller was presented in [23]. The PID controller was tuned with differential evolution optimization (DEO), grey wolf optimization (GWO) and grasshopper optimization (GOA) algorithms. Integral absolute error (IAE), integral square error (ISE) and integral time absolute error (ITAE) were used as performance indices. The interleaved buck-boost converter was controlled with PID, and the coefficients were optimized with PSO algorithm [24].

PID, FOPID, and TID (tilt-integral-derivative) controllers were used to operate a buck type step-down converter in this study. The coefficients of these controllers have been optimized for the first time with the Fitness-Distance Balance Based Runge Kutta (FDBRUN) [25] algorithm in the literature and presented in comparison with the results of the Aquila Optimizer (AO) [26], African Vultures Optimization Algorithm (AVOA) [27] and Hunger Games Search (HGS) [28] optimization algorithms. The *S*-domain circuit model of the circuit is derived in order to employ these optimization approaches. The controller coefficients derived by four distinct optimization approaches are used to evaluate the converter response, and the results are presented.

In the second part of the study, the mathematical equations and modeling of the buck converter are presented. FOPID and TID controllers used in closed loop control algorithm are

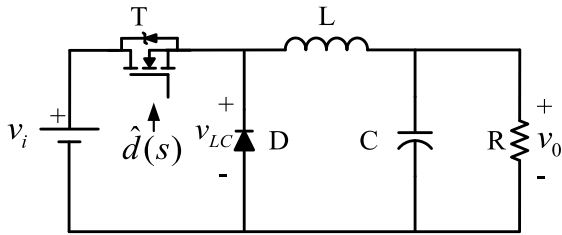


FIGURE 1. Buck converter topology.

explained in Section 3. In Section 4, FDBRUN algorithm, which is the metaheuristic optimization algorithm proposed in the study is mentioned. The simulation study with different optimization algorithms and controllers is given in Section 5 and the obtained results are given in Section 6.

II. MODELING OF BUCK CONVERTER

Because switched-mode power supplies are more efficient, they have many applications such as television, electric vehicles, mobile devices, and uninterruptible power supply. Buck converter, which is switched-mode power supply have a variety of applications and is used to decrease the DC voltage level. The converter, which is made up of passive parts like inductors and capacitors as well as switching elements like MOSFETs and diodes is controlled by modifying the MOSFET's duty cycle. The voltage waveform produced by high-frequency switching is filtered by the LC filter at the output, a constant DC voltage is obtained.

When the PWM signal is applied to the MOSFET in the converter, the input voltage is also applied to the LC filter. The voltage created on the LC filter ends as a result of switching the MOSFET is seen in Fig. 2a. It is seen that the LC filter voltage, which is a square wave takes the value of the input voltage when the switch is turned on and becomes zero when the switch is turned off. Simultaneously, when voltage is applied, the inductance current increases, and when no voltage is applied, the current reduces. Inductance current and output voltage vary depending on the duty cycle of the switching signal as seen in Fig. 2b and Fig. 2c.

Because it is a switched-type converter, the buck converter circuit seen in Fig. 1 is classified as a nonlinear system. Different circuit equations occur and electrical quantities change depending on the conduction state of the semiconductor switch positioned at the input part of the circuit. While the switch is turned on, energy is stored in the inductance while the output is supplied. When the switch is turned off, the energy stored in the inductance is delivered into the output. The energy balance is accomplished and the desired output is obtained by applying the duty cycle computed by the control algorithm.

Firstly, the system must be linearized before designing the converter's control. The dynamic equations of the buck converter used to make the system linear are given in equations (1) and (2). In these equations, V_i is the input voltage, v_0 is the output voltage, L is the inductance, C is the output capacitor, R is the output load resistance, and d is

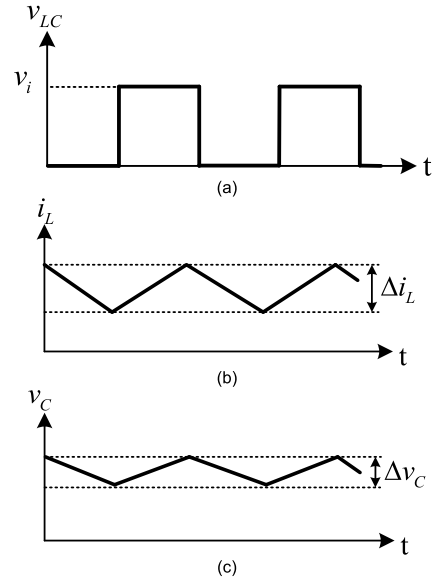


FIGURE 2. Buck converter waveforms: (a) LC filter voltage, (b) Inductor current, (c) Output voltage.

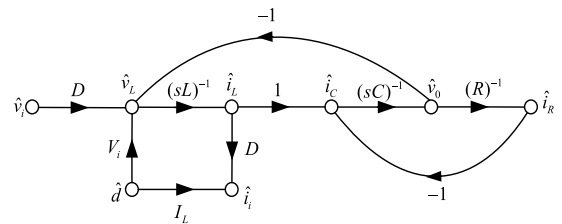


FIGURE 3. Small-signal model of the buck converter.

the switching state. When writing the equations, the circuit equations that occur when the switch is turned on and off are employed. The state variables in these equations are inductance current and capacitor voltage. The transfer function of the converter can be calculated using these equations.

$$\frac{di_L}{dt} = -\frac{v_0}{L} + d \times \frac{V_i}{L} \tag{1}$$

$$\frac{dv_0}{dt} = \frac{i_L}{C} - \frac{v_0}{R \times C} \tag{2}$$

Fig. 3 depicts the converter's signal-flow graph theory flow. The transfer function of the converter to be investigated can be obtained using this flow.

The s -domain transfer function of the converter obtained by using equations is given in equation (3). The study examines the performances of different control structures in different optimization techniques utilizing this transfer function, which gives the fluctuation of the output voltage based on the duty cycle.

$$G(s) = \frac{\hat{v}_o}{\hat{d}} = V_i \frac{\frac{1}{L \times C}}{s^2 + s \frac{1}{R \times C} + \frac{1}{L \times C}} \tag{3}$$

Equations (4) and (5) can be used to compute the minimal inductance and capacitor value that should be used based on the ripple amount (i_L) and switching frequency (f_s) determined while designing the buck converter. As the equations

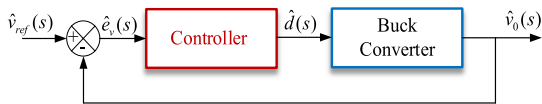


FIGURE 4. Control block diagram of the converter.

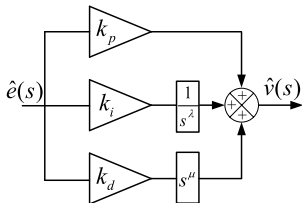


FIGURE 5. FOPID block diagram.

show, increasing the switching frequency causes the inductance and capacitor values for the same current and voltage ripple to decrease.

$$L_{\min} = \frac{(V_i - V_0) \times D}{2 \times \Delta i_L \times f_s} \quad (4)$$

$$C_{\min} = \frac{\Delta i_L}{8 \times f_s \times \Delta v} \quad (5)$$

III. CLOSED-LOOP CONTROLLED BUCK CONVERTER

Open-loop and closed-loop control are the two basic control architectures of converters. If a regulation is not required, open-loop control is applied. It can control the system if each electrical quantity is stable. However, output voltage of the converter changes when a disturbance occurs in the system. To regulate the output, closed-loop control structure is required. Fig. 4 depicts the closed-loop control block diagram of the converter. In the figure, $\hat{v}_0(s)$, $\hat{v}_{ref}(s)$, $\hat{e}_v(s)$ ve $\hat{d}(s)$ defines output voltage, reference value of output voltage, voltage error and duty cycle, respectively. The controller attempts to reduce the output voltage error to zero while ensuring that the desired output voltage is reached.

There are various types of regulators used in closed loop control. In this study, PID, FOPID and TID regulators were examined.

A. FRACTIONAL ORDER PROPORTIONAL INTEGRAL DERIVATIVE (FOPID) CONTROLLER

The FOPID controller transfer function is given in (6). In the equation, k_p , k_i , k_d , λ and μ define the proportional constant, integral constant, derivative constant, integral order and fractional derivative order, respectively. In Fig. 5, the block diagram of FOPID controller is seen. The reference signal is obtained by summing the results obtained by passing the error value of the control signal through proportional, integral, and derivative blocks.

$$G_{FOPID}(s) = k_p + \frac{k_i}{s^\lambda} + k_d s^\mu \quad (\lambda, \mu > 0) \quad (6)$$

If the integral order and fractional derivative order is $\lambda = 1$ and $\mu = 1$, $\lambda = 0$ and $\mu = 1$, $\lambda = 1$ and $\mu = 0$, $\lambda = 0$ and $\mu = 0$, PID, PD, PI and P controller are obtained, respectively. A generalized FOPID control extends

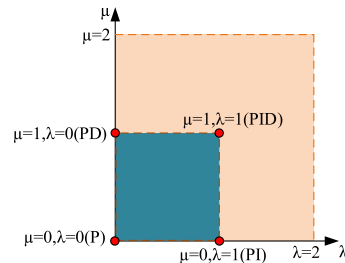


FIGURE 6. FOPID controller plane.

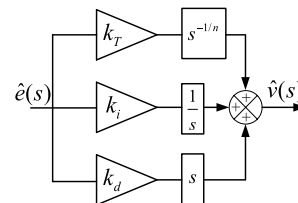


FIGURE 7. TID controller block diagram.

PID control from a point to a plane in Fig. 6, which shows the relationship between FOPID and classical controllers. Controllers that are formed depending on the values of μ and λ parameters are seen in the figure.

B. TILT INTEGRAL DERIVATIVE (TID) CONTROLLER

The TID controller is a compensator with coefficients of k_T , k_i , k_d and tuning parameter of n . TID controller, which has a similar structure with PID controller, has $s^{-1/n}$ transfer function with n parameter and k_T parameter instead of proportional coefficient k_p .

IV. THE PROPOSED METAHEURISTIC OPTIMIZATION ALGORITHM

A. RUNGE KUTTA OPTIMIZATION ALGORITHM

The RUN algorithm was presented to the literature by [25] in 2021 as a new swarm-based optimization algorithm with stochastic components. To get the best value, the researchers employed the slope formula in the algorithm as a search logic for all solution candidates in the population. The algorithm consists of two stages: the search strategy using the Runge-Kutta theory and the improvement of the solution quality. The basic structure of the RUN algorithm will be explained in the subsections of this section.

1) INITIALIZATION POPULATION

The first part of the RUN algorithm is defined as the creation of the initial population in order to find the most suitable solution candidate. The initial population is formed between the minimum and maximum limit values of the control variables determined by the researcher. The initial population is expressed mathematically as in (7).

$$x_{n,i} = L_i + rand \times (U_i - L_i) \quad (7)$$

n represents each solution candidate in the population ($n = 1, 2, 3, \dots, N$). N represents the number of randomly generated solution candidates within the limit values, in other words, the size of the population. L_i and U_i show the limit

values of the i_{th} variable ($i = 1, 2, 3, \dots, D$). $rand$ represents a randomly generated number between $[0,1]$.

2) UPDATING SOLUTIONS

The algorithm starts the optimization process with the candidate solutions created in the initial population. At each iteration, the candidate solutions use a search mechanism (SM) based on the Runge-Kutta technique to update their locations for the next iteration. The SM method plays an active role in providing global (discovery) and local (exploitation) search. This situation is given in detail in algorithm 1.

Algorithm 1 Exploration and Exploitation Phases in RUN Algorithm

```

if rand < 0.5
    exploration phase
     $x_{n+1} = (x_c + r \times SF \times g \times x_c) + SF \times SM + \mu \times x_s$ 
else
    exploitation phase
     $x_{n+1} = (x_m + r \times SF \times g \times x_m) + SF \times SM + \mu \times x_{ss}$ 
end
    
```

The r and g used in algorithm 1 represents an integer number as 1 or -1 , and a random number between $[0,2]$, respectively. μ defines a random number and is calculated based on equation (8). The expression $randn$ in equation (8) represents a random number with normal distribution. x_s ve x_{ss} expressions are explained mathematically as seen in equation (9). x_m ve x_c are formulated as in equation (10).

$$\mu = 0.5 + 0.1 \times randn \tag{8}$$

$$x_s = randn \times (x_m - x_c)$$

$$x_{ss} = randn \times (x_{r1} - x_{r2}) \tag{9}$$

$$x_c = \varphi \times x_n + (1 - \varphi) \times x_{r1}$$

$$x_m = \varphi \times x_{best} + (1 - \varphi) \times x_{best} \tag{10}$$

φ is expressed as a random number in the range $[0,1]$. x_{best} is defined as the best solution so far, while x_{best} is defined as the best solution obtained from each iteration. While SF is defined as the adaptive factor that provides the balance between exploration and exploitation, it is shown mathematically as in equation (11).

$$SF = 2 \times (0.5 - rand) \times (a \times e^{(-b \times rand \times \frac{i}{Maxi})}) \tag{11}$$

In the equation, a and b defines two constant number, i defines current iteration number, and $Maxi$ defines maximum iteration number.

3) ENHANCED SOLUTION QUALITY

The enhanced solution quality (ESQ) method in this section is employed to prevent the solution candidates used in the optimization process from being caught in local solution points or solution traps and to increase the solution quality.

The calculation of x_{new2} according to this method is shown in detail in algorithm 2. In the method, a random number of w and $rand$ are used together. The ESQ method runs while $rand < 0.5$, and $x_{new2} = x_{new1} + r \times w \cdot |(x_{new1} - x_{avg}) + randn|$ equation is used if $w < 1$, otherwise $x_{new2} = (x_{new1} - x_{avg}) + r \times w \times |(u \times x_{new1} - x_{avg}) + randn|$ is applied to enhance the solution [29].

Algorithm 2 Calculation of the x_{new2} via the Enhanced Solution Quality Method

```

if rand < 0.5
    if w < 1
         $x_{new2} = x_{new1} + r \times w \times |(x_{new1} - x_{avg}) + randn|$ 
    else
         $x_{new2} = (x_{new1} - x_{avg}) + r \times w \times |(u \cdot x_{new1} - x_{avg}) + randn|$ 
    end
end
    
```

w , x_{avg} and x_{new1} are, respectively, defined as a random number, the average of three random solutions and a new solution, and given in equation (12)-(14).

$$w = rand(0, 2) \times e^{(-c \times (\frac{i}{Maxi}))} \tag{12}$$

$$x_{avg} = \frac{x_{r1} + x_{r2} + x_{r3}}{3} \tag{13}$$

$$x_{new1} = \beta \times x_{avg} + (1 - \beta) \times x_{best} \tag{14}$$

The variable β expresses a random number between $[0,1]$. r is an integer that gets number of 1,0 or -1 . c is calculated using the equation of $c = 0.5 \times rand$. If the solution x_{new2} does not have a better solution than the current solution candidates, x_{new3} is calculated, which allows the better candidate solutions shown in algorithm 3 to be obtained.

Algorithm 3 Calculation of the x_{new3}

```

if rand < w
     $x_{new3} = (X_{new2} - randx_{new2}) + SF (randx_{RK} + (v \times x_b - x_{new2}))$ 
end
    
```

The parameter of v is calculated by the equation of $v = 2 \times rand$.

B. THE PROPOSED METHOD: FITNESS DISTANCE BALANCE-BASED RUN ALGORITHM

Metaheuristic optimization algorithms are caught in local solution traps in the search process life cycle to find the most suitable solution. In order to eliminate this undesirable situation, [30] presented a method called fitness distance balance (FDB) to the literature in 2020. In this method, it is aimed to better select the solution candidates that guide the search process by using fitness values. Cengiz et al. used the FDB selection method to eliminate the disadvantage of RUN algorithm being caught in local solution traps. The fitness values of the solution candidates and their distance

from the best solution candidate (P_{best}) in the population are considered in the FDB selection process. FDB selection method is applied according to the following process steps [31], [32], [33], [34], [35].

- i. Optimization algorithms consist of n -unit candidate solution spaces to solve the optimization problem. The vector of solution candidates (population, P) in the solution space and the vector of fitness values (F) of these candidates are shown in equation (15).

$$P = \begin{bmatrix} p_1 \\ \vdots \\ p_2 \end{bmatrix} = \begin{bmatrix} x_{11} & \cdots & x_{1m} \\ \vdots & \ddots & \vdots \\ x_{n1} & \cdots & x_{nm} \end{bmatrix}_{n \times m},$$

$$F = \begin{bmatrix} f_1 \\ \vdots \\ f_n \end{bmatrix}_{n \times 1} \quad (15)$$

- ii. The Euclidean distance of the i -th candidate solution p_i in the population to the best solution candidate p_{best} is expressed as in equation (16).

$$\begin{aligned} & \sqrt{\sum_{i=1}^n P_i, D_{P_i}} \\ &= \sqrt{(p_{i[1]} - p_{best[1]})^2 + (p_{i[1]} - p_{best[1]})^2} \\ & \times \sqrt{\cdots + (p_{i[m]} - p_{best[m]})^2} \end{aligned} \quad (16)$$

- iii. The distance of solution candidates in the population from p_{best} is represented by the vector D_p given in equation (17).

$$D_p \equiv \begin{bmatrix} d_1 \\ \vdots \\ d_n \end{bmatrix}_{n \times 1} \quad (17)$$

- iv. In the calculation of the FDB value, normalization is required so that the vector of fitness values and distance values of the solution candidates do not dominate each other. Normalized fitness and distance values between [0, 1] are used to calculate the FDB values (S_p) of the solution candidates as $normF$ and $normD_p$, respectively.

$$\sum_{i=1}^n P_i, S_{P[i]} = w * normF_{[i]} + (1-w) * normD_{P[i]} \quad (18)$$

In equation (18), w is expressed as the weight coefficient representing the effects of the fit and distance parameters on the FDB value, and the w coefficient is accepted as 0.5.

- v. The FDB values of the solution candidates in the solution space of the optimization problem are represented as the n -dimensional S_p vector as in equation (19).

$$S_p \equiv \begin{bmatrix} s_1 \\ \vdots \\ s_n \end{bmatrix}_{n \times 1} \quad (19)$$

TABLE 1. Buck converter parameters.

Symbol	Quantity	Value
v_i	input voltage	16 V
v_o	output voltage	12 V
f_s	switching frequency	15 kHz
L	inductor	1.1 mH
C	capacitor	84 μ F
R	load	11 Ω

TABLE 2. The lower and upper limits of the controllers.

PID	FOPID	TID
$1 \leq k_p \leq 50$	$1 \leq k_p \leq 50$	$0.01 \leq k_t \leq 100$
$1 \leq k_i \leq 10$	$0.01 \leq k_i \leq 10$	$0 \leq n \leq 1$
$1 \leq k_d \leq 0.001$	$1 \leq \lambda \leq 2$	$0.1 \leq k_i \leq 50$
	$0 \leq k_{it} \leq 0.001$	$0.001 \leq k_{it} \leq 0.01$
	$0 \leq \mu \leq 2$	

After the S_p vector showing the FDB scores of the solution candidates in the solution space of the optimization problem is created, the roulette wheel method is used to select the solution candidates to guide the search process to reach the global solution point. The point where the FDB selection method is applied is given in equation (20) [36].

$$x_{avg} = \begin{cases} X(fdb, :) + X(fdb, :) + X(fdb, :)/3; & rand < 0.7 \\ & (X(A, :) + X(B, :) + X(C, :))/3; & rand \geq 0.7 \end{cases} \quad (20)$$

The flowchart of FDBRUN algorithm is shown in Fig. 8.

V. SIMULATION RESULTS

In this section, comparative simulation results of buck converter with PID, FOPID and TID control structures, optimal parameters determined by FDBRUN, AO, AVOA, and HGS optimization algorithms, are presented. Table 1 shows the circuit parameters of the buck converter. The transfer functions given in (22)-(25), as shown at the bottom of the next page, are derived depending on the parameters.

A. DESIGN OF THE DIFFERENT CONTROLLER STRUCTURES VIA METAHEURISTIC ALGORITHMS

Controllers used in power electronics converters are expected to dampen the oscillations that occur in sudden changes in the system and minimize the steady state error. In order to achieve this, the optimization of the controller coefficients has an important role. The objective function used in any optimization method is also important for better results. The objective function given in (21) was preferred in the study because it provides fast dynamic response, low overshoot, short settling time and minimum steady-state error in sudden changing system operating conditions. The function [37] was firstly used in [38] for automatic voltage regulator.

$$J = (1 - e^{-\alpha}) \times (E_{ss} + M_p) + e^{-\alpha} \times (T_s - T_r) \quad (21)$$

In this equation, α is defined as the weight coefficient often set to 1, E_{ss} defines the steady-state error, the percent

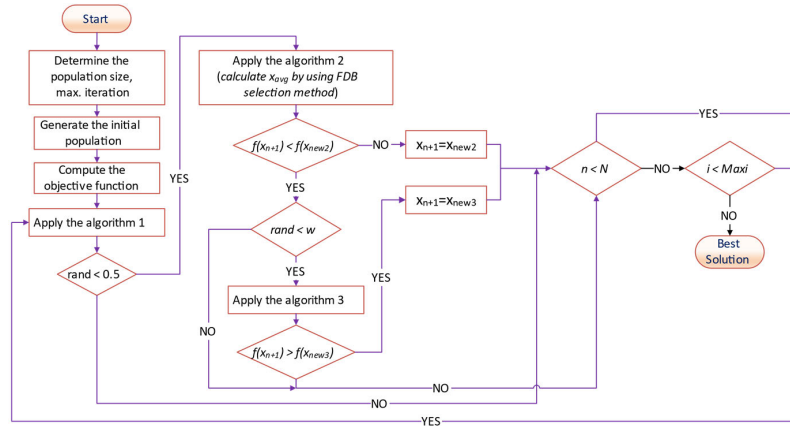


FIGURE 8. Flowchart of the FDBRUN algorithm.

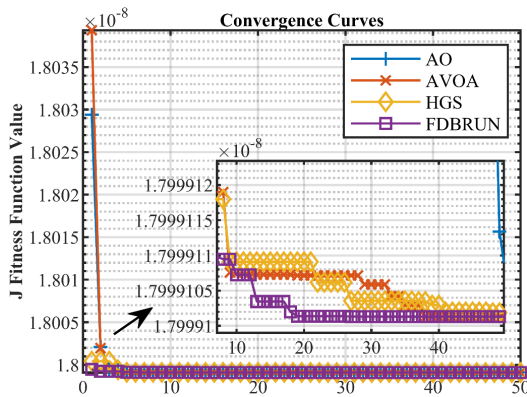


FIGURE 9. Curves of convergence profiles of FDBRUN algorithm.

TABLE 3. Optimized parameters of the PID, FOPID and TID controllers.

Controller	Parameter	Algorithm			
		FDBRUN	AO	AVOA	HGS
PID	k_p	9.9944	9.9946	9.9946	9.9944
	k_i	0.1039	9.6392	4.6443	0.1000
	k_d	0.0010	0.0010	0.0010	0.0010
FOPID	k_p	45.3617	15.9003	22.8459	49.8597
	k_i	0.1864	7.7065	5.6190	2.5693
	λ	0.0779	0.2844	0.04383	0.0020
	k_d	9.1648×10^{-4}	0.0010	5.8431×10^{-4}	1×10^{-3}
	μ	1.7506	1.6619	1.7841	1.7568
TID	k_r	3.6490	11.8373	99.9969	4.1335
	N	0.5689	0.5703	0.5688	0.7070
	k_i	7.5609	29.7427	11.6809	39.4125
	k_d	0.0100	0.0100	0.0100	0.0062

overshoot is expressed as M_p , T_s defines the time to settle in a band gap of $\pm 2\%$, and T_r defines the rise time. In optimization problems, it is necessary to determine the limits of the variables defined as control variables. In this study, the minimum and maximum limit values of PID, FOPID and TID controller parameters are used as in Table 2 [16].

Fig. 9 shows convergence profile of best runs of the proposed FDBRUN algorithm for FOPID controller. As seen from Fig. 9, the proposed FDBRUN algorithm converges to the lowest fitness function value.

To ensure fair performance comparison, the number of iterations as the stopping criterion and population size is set to 50 and 25 respectively for each optimization algorithm. During the determination of the controller parameters, all

optimization algorithms are run 30 times. The optimal controller parameters found by the optimization algorithms are given in Table 3. When the values in Table 3 are examined in detail, it is seen that the optimized controller parameters are within the limit values in Table 2. The results obtained at the end of 30 trials are statistically evaluated in Table 4.

The FOPID controller structure utilized in the buck converter structure may be expressed as the structure with the best objective function for each optimization technique according to the PID and TID controllers when Table 4 is reviewed in detail. As can be seen from the boxplot shown in Fig. 10, the statistical performance of the FDBRUN optimization algorithm in all controllers is better than the performance of other AO, AVOA and HGS algorithms.

$$TF_{AO(s)} = \frac{1.7316 \times 10^5 s^{1.9463} + 2.7533 \times 10^9 s^{0.2844} + 1.3345 \times 10^9}{s^{2.2844} + 1.7316 \times 10^5 s^{1.9463} + 1082.3 s^{1.2844} + 2.7641 \times 10^9 s^{0.2844} + 1.3345 \times 10^9} \quad (22)$$

$$TF_{AVOA(s)} = \frac{1.587 \times 10^5 s^{1.862} + 7.8548 \times 10^9 s^{0.0779} + 3.2277 \times 10^7}{s^{2.0779} + 1.587 \times 10^5 s^{1.862} + 1082.3 s^{1.0779} + 7.8657 \times 10^9 s^{0.0779} + 3.2277 \times 10^7} \quad (23)$$

$$TF_{FDBRUN(s)} = \frac{1.587 \times 10^5 s^{1.862} + 7.8548 \times 10^9 s^{0.0779} + 3.2277 \times 10^7}{s^{2.0779} + 1.587 \times 10^5 s^{1.862} + 1082.3 s^{1.0779} + 7.8657 \times 10^9 s^{0.0779} + 3.2277 \times 10^7} \quad (24)$$

$$TF_{HGS(s)} = \frac{1.7316 \times 10^5 s^{1.7588} + 8.6337 \times 10^9 s^{0.002} + 4.449 \times 10^8}{s^{2.002} + 1.7316 \times 10^5 s^{1.7588} + 1082.3 s^{1.002} + 8.6445 \times 10^9 s^{0.002} + 4.449 \times 10^8} \quad (25)$$

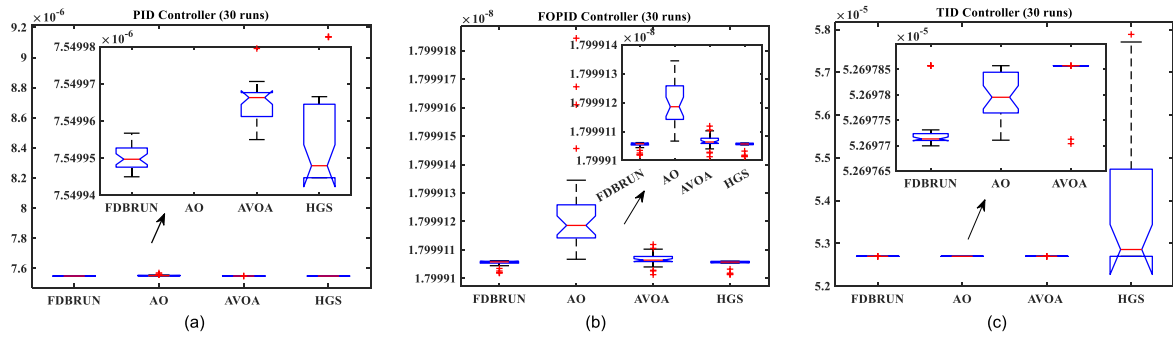


FIGURE 10. Box plots of the optimization algorithms for the (a) PID, (b) FOPID and (c) TID controllers.

TABLE 4. Minimum, mean, maximum and standard deviation values for each operating condition.

Algorithm	Controller	Minimum	Mean	Maximum	Standard Deviation
FDBRUN	PID	7.5499×10^{-6}	7.55×10^{-6}	7.55×10^{-6}	3.1548×10^{-12}
	FOPID	1.7999×10^{-8}	1.7999×10^{-8}	1.7999×10^{-8}	1.346×10^{-15}
	TID	5.2698×10^{-5}	5.2698×10^{-5}	5.2698×10^{-5}	5.5086×10^{-11}
AO	PID	7.55×10^{-6}	7.5541×10^{-6}	7.5706×10^{-6}	4.4304×10^{-9}
	FOPID	1.7999×10^{-8}	1.7999×10^{-8}	1.7999×10^{-8}	1.7909×10^{-15}
	TID	5.2698×10^{-5}	5.2698×10^{-5}	5.2698×10^{-5}	4.4115×10^{-11}
AVOA	PID	7.55×10^{-6}	7.55×10^{-6}	7.55×10^{-6}	7.2444×10^{-12}
	FOPID	1.7999×10^{-8}	1.7999×10^{-8}	1.7999×10^{-8}	2.2854×10^{-15}
	TID	5.2698×10^{-5}	5.2698×10^{-5}	5.2698×10^{-5}	3.7897×10^{-11}
HGS	PID	7.5499×10^{-6}	7.7087×10^{-6}	9.1373×10^{-6}	4.8434×10^{-7}
	FOPID	1.7999×10^{-8}	1.7999×10^{-8}	1.7999×10^{-8}	1.5238×10^{-15}
	TID	5.2698×10^{-5}	5.3979×10^{-5}	5.7885×10^{-5}	1.8249×10^{-6}

In the case of using FOPID as the controller in the system shown in Fig. 4, the coefficients determined by the AO, AVOA, FDBRUN and HGS algorithms and the transfer functions obtained using the system parameters seen in Table 1 are given in the equations (22)-(25), respectively.

1) TRANSIENT RESPONSE ANALYSIS OF THE BUCK CONVERTER

During the optimization process, the best parameters of PID, FOPID, and TID controllers are obtained using FDBRUN, AO, AVOA, and HGS algorithms. The time responses of the buck converter according to the obtained controller parameters are shown in Fig. 11. Furthermore, Table 5 describes the transient response criteria in detail, including overshoot, rise time, settling time, and peak time. According to these values, it is seen that the FDBRUN based FOPID controller is better than other controllers in improving the transient response of the buck converter system.

2) FREQUENCY RESPONSE AND COMPARISON ANALYSIS OF THE PERFORMANCE INDICES

The bode diagram that shows gain and phase margin of the FOPID controller which parameters are determined by optimization algorithms is given in Fig. 12. In addition, integral absolute error (IAE) [39], integral square error (ISE) [40], integral time absolute error (ITAE) [41] and integral time squared error (ITSE) [42] performance indices are used to evaluate the performance of the algorithms in more detail. The formulas of the indices are given in

TABLE 5. Transient response analysis results of the system via the PID, FOPID and TID controllers.

Controller	Transient response	Algorithm			
		FDBRUN	AO	AVOA	HGS
PID	Peak value (V)	12.4559	12.4560	12.4559	12.4559
	Overshoot (%)	3.4725	3.4725	3.4726	3.4725
	Rise time (10^{-5} s)	1.1285	1.1285	1.1285	1.1285
	Settling time (10^{-5} s)	8.0246	8.0246	8.0247	8.024
	Peak time (10^{-5} s)	3.5750	3.5750	3.5750	3.575 ⁵
FOPID	Peak value (V)	11.9994	11.9986	11.9988	11.9993
	Overshoot ($\%10^{-5}$)	1.4015	2.0300	0.77346	0.1647
	Rise time (10^{-9} s)	8.0031	8.0233	8.0078	8.004 ⁹
	Settling time (10^{-9} s)	9.8038	9.8285	9.8096	9.805
	Peak time (10^{-5} s)	9.8220	9.9920	9.8750	9.860
TID	Peak value (V)	11.9925	11.9998	11.9920	11.9867
	Overshoot (%)	0.0000	0.0046	0.0381	0.9186
	Rise time (10^{-6} s)	1.3753	1.3784	1.3728	2.076
	Settling time (10^{-6} s)	2.4506	2.4677	2.4374	3.469
	Peak time (10^{-6} s)	0.001	0.09986	7.8008	0.1130

the equations (26)-(29).

$$IAE = \int_0^T |e(t)| dt \tag{26}$$

$$ISE = \int_0^T e^2(t) dt \tag{27}$$

$$ITAE = \int_0^T t |e(t)| dt \tag{28}$$

$$ITSE = \int_0^T t e^2(t) dt \tag{29}$$

T is the simulation time, and e(t) is the error signal, according to these equations. Performance indexes are examined in two stages. In the first stage, the response of the system under unchanged conditions is examined, while in the second stage, the system response is examined in case of changes in resistance (R), inductance (L) and capacitance (C) values.

The results of the performance indices according to the system response of the FOPID controller under continuous conditions are shown in Fig. 13 as a bar graph. The numer-

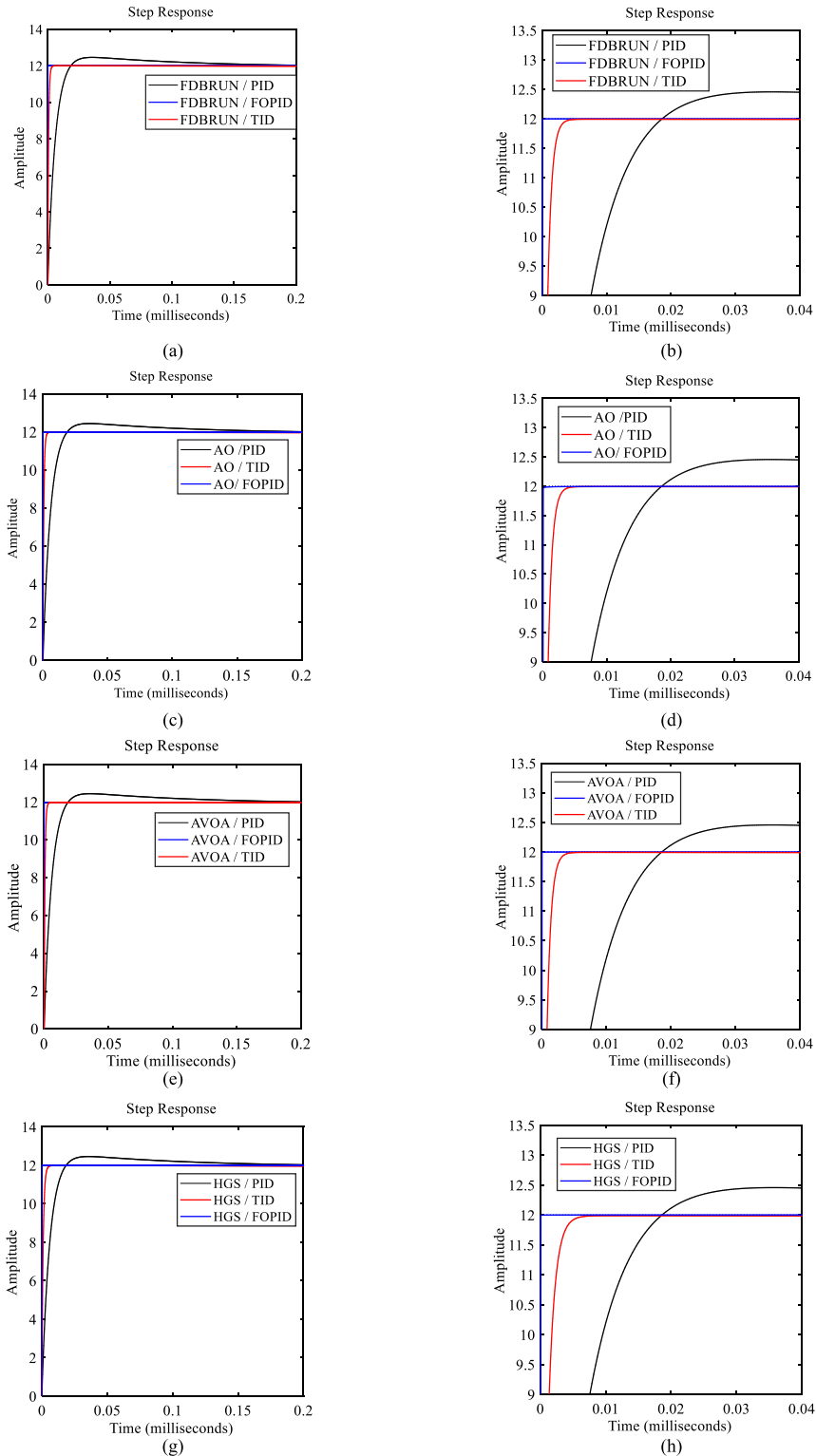


FIGURE 11. Comparative step response analysis of the buck converter system: (a) FDBRUN (steady-state), (b) FDBRUN (transient), (c) AO (steady-state), (d) AO (transient), (e) AVOA (steady-state), (f) AVOA (transient), (g) HGS (steady-state), (h) HGS (transient).

ical values of the performance indices are given in Table 6. Under continuous working conditions, the FDBRUN algorithm has the best value in all performance indexes, according to Table 6. In other words, the FDBRUN algorithm for the

IAE performance index has 9.8101%, 0.7911%, and 1.0284% less values than the AO, AVOA, and HGS algorithms.

Fig 14 shows the results of the performance indices according to the system response of the FOPID controller depending

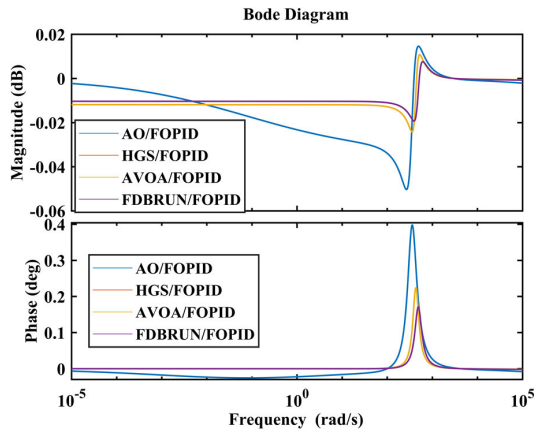


FIGURE 12. Bode plot of the buck converter system with a FOPID controller adjusted via FDBRUN, AO, AVOA, and HGS algorithms.

on the change of the R-L-C parameters. According to the change of R-L-C parameters, FDBRUN algorithm is seen as the algorithm with the best value among the performance indexes in Table 6. In addition, the FDBRUN algorithm has 33.4250%, 2.0632% and 3.2324% less values than the AO, AVOA, and HGS algorithms, respectively for the IAE performance index.

TABLE 6. Performance indices results for operating conditions.

Algorithm	Continuous operating conditions			
	IAE	ITAE	ISE	ITSE
AO	0.1388×10^{-5}	0.7894×10^{-11}	0.1470×10^{-4}	0.1273×10^{-13}
AVOA	0.1274×10^{-5}	0.3244×10^{-11}	0.1450×10^{-4}	0.0178×10^{-13}
FDBRUN	0.1264×10^{-5}	0.2944×10^{-11}	0.1440×10^{-4}	0.0174×10^{-13}
HGS	0.1277×10^{-5}	0.3466×10^{-11}	0.1450×10^{-4}	0.0238×10^{-13}
Algorithm	Change of RLC parameters			
	IAE	ITAE	ISE	ITSE
AO	0.1940×10^{-5}	0.3064×10^{-10}	0.1481×10^{-4}	0.1927×10^{-12}
AVOA	0.1484×10^{-5}	0.1179×10^{-10}	0.1460×10^{-4}	0.0268×10^{-12}
FDBRUN	0.1454×10^{-5}	0.1149×10^{-10}	0.1440×10^{-4}	0.0266×10^{-12}
HGS	0.1501×10^{-5}	0.1340×10^{-10}	0.1470×10^{-4}	0.0362×10^{-12}

VI. CONCLUSION

In this study, the performance of buck type step-down converter with PID, FOPID and TID controllers is investigated. The coefficients, which determines the performances of the controllers are determined by AO, AVOA, FDBRUN and HGS optimization methods. FDBRUN method is used for the first time to optimize the PID controller in the buck converter in the literature. When the steady state response of the buck system is examined, the FOPID control structure has the best objective function, and the best control response is obtained

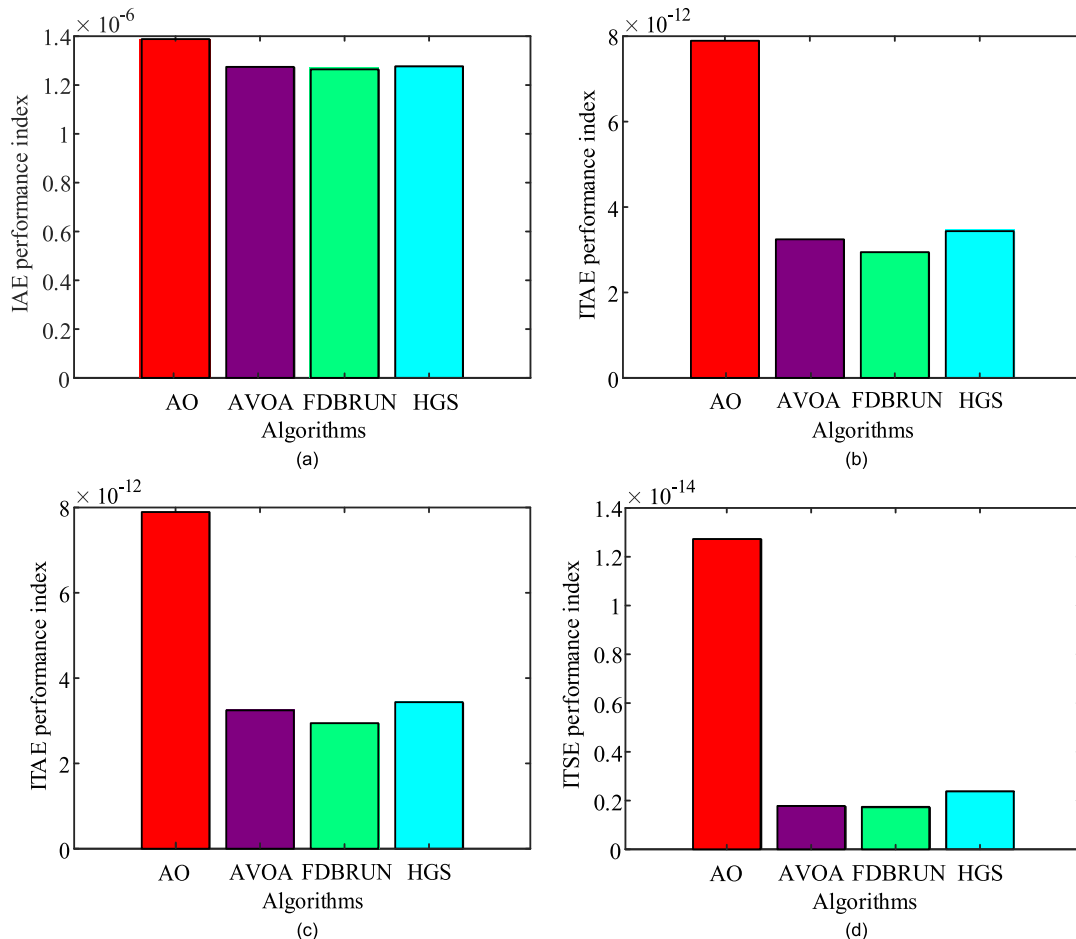


FIGURE 13. Performance indices of algorithms for continuous operating conditions: (a) IAE, (b) ITAE, (c) ISE, (d) ITSE.

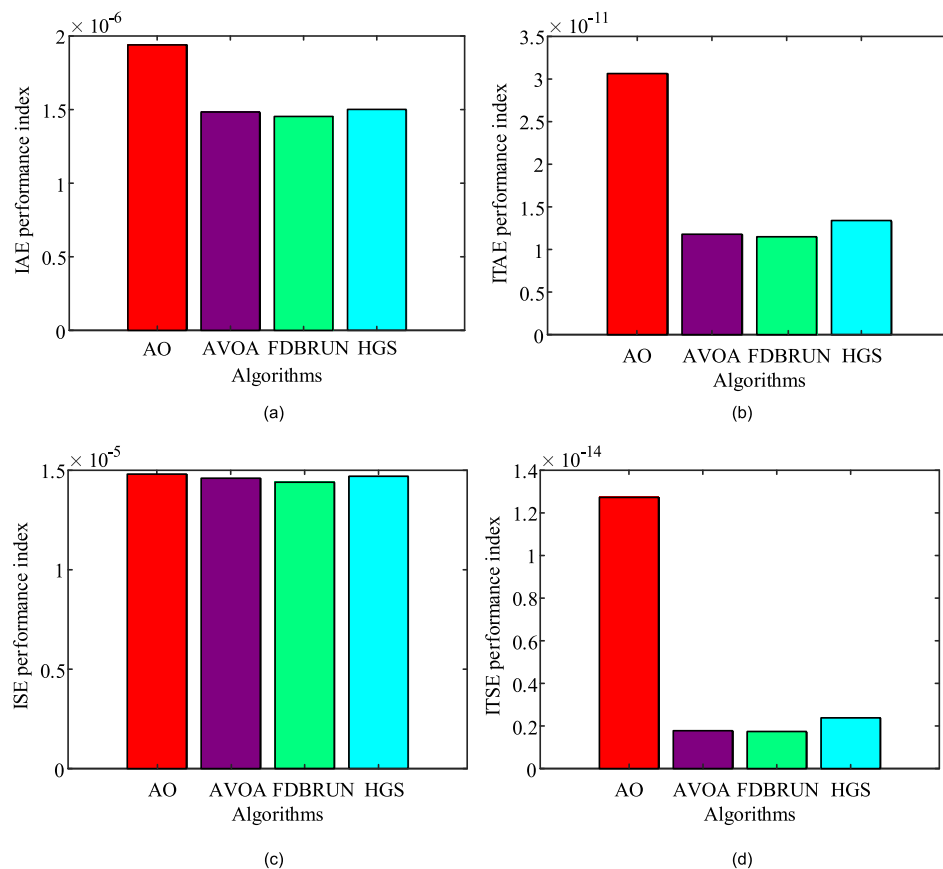


FIGURE 14. Performance indices of algorithms for the conditions for changing RLC parameters: (a) IAE, (b) ITAE, (c) ISE, (d) ITSE.

with the coefficients determined by the FDBRUN optimization method. In the transient performance, the FOPID controller, the coefficients of which are determined by the FDBRUN optimization method, give the best response in the parameters of transient peak value, percent overshoot, rise time, settling time and time to peak value. When the robustness of the algorithms is examined in detail in terms of performance indices, the FDBRUN algorithm has the best value in terms of performance indices calculated depending on the controller parameters optimized by the optimization algorithms in steady state conditions. It is seen that the FDBRUN algorithm has the best value among the optimization algorithms according to the performance indices after the change of the R-L-C values in the system parameters. As a result of the coefficient optimization, which is made with the FDBRUN algorithm, the FOPID controller provides the best performance in the system response. The results reveals that the FDBRUN method achieves best performance compared to other tested methods, and is applicable for coefficient optimization in power electronics converter controller.

REFERENCES

- [1] R. I. Kayaalp, T. Demirdelen, and M. Tumay, "A novel fuzzy logic control for bidirectional DC-DC converter and comparison with dual phase-shift control method in medium voltage applications," in *Proc. IEEE Int. Conf. Comput. Intell. Virtual Environ. Meas. Syst. Appl. (CIVEMSA)*, Jun. 2016, pp. 1–6.
- [2] S. Mobayan, F. Bayat, C. C. Lai, A. Taheri, and A. Fekih, "Adaptive global sliding mode controller design for perturbed DC-DC buck converters," *Energies*, vol. 14, pp. 1–12, Feb. 2021.
- [3] Z. Shen and S. Zhong, "An improved hysteresis voltage mode of synchronous rectifier buck circuit," *IEEE Access*, vol. 8, pp. 121022–121032, 2020.
- [4] A. Iskhakov, Y. Portnoy, S. Skovpen, and D. Gladkiy, "Directbeat control of a buck converter," in *Proc. 45th Annu. Conf. IEEE Ind. Electron. Soc. (IECON)*, Oct. 2019, pp. 347–352.
- [5] C.-N. Huang and A. Chung, "An intelligent design for a PID controller for nonlinear systems," *Asian J. Control*, vol. 18, no. 2, pp. 447–455, Nov. 2014.
- [6] A. Khalilian, G. Sahamijoo, O. Avatefipour, F. Piltan, and M. R. S. Nasrabad, "Design high efficiency-minimum rule base PID like fuzzy computed torque controller," *Int. J. Inf. Technol. Comput. Sci.*, vol. 6, no. 7, pp. 77–87, Jun. 2014.
- [7] S. M. Ghamari, H. G. Narm, and H. Mollaei, "Fractional-order fuzzy PID controller design on buck converter with antlion optimization algorithm," *IET Control Theory Appl.*, vol. 16, no. 3, pp. 340–352, Dec. 2021.
- [8] U. M. Nath, C. Dey, and R. K. Mudi, "Fuzzy rule-based auto-tuned internal model controller for real-time experimentation on temperature and level processes," *Int. J. Autom. Control*, vol. 14, no. 2, pp. 239–256, Feb. 2020.
- [9] J. Hao and G. Zhang, "Data-driven tracking control for a class of unknown nonlinear time-varying systems using improved PID neural network and Cohen-Coon approach," in *Proc. IEEE 10th Data Driven Control Learn. Syst. Conf.*, May 2021, pp. 619–624.
- [10] A. A. Azman, M. H. F. Rahiman, N. N. Mohammad, M. H. Marzaki, M. N. Taib, and M. F. Ali, "Modeling and comparative study of PID Ziegler Nichols (ZN) and Cohen-Coon (CC) tuning method for multi-tube aluminum sulphate water filter (MTAS)," in *Proc. IEEE 2nd Int. Conf. Autom. Control Intell. Syst. (I2CACIS)*, Oct. 2017, pp. 25–30.
- [11] C. I. Muresan and R. De Keyser, "Revisiting Ziegler-Nichols. A fractional order approach," *ISA Trans.*, vol. 129, pp. 287–296, Oct. 2022.

- [12] I. Al-Wesabi, Z. Fang, H. M. H. Farh, A. A. Al-Shamma'a, A. M. Al-Shaalan, T. Kandil, and M. Ding, "Cuckoo search combined with PID controller for maximum power extraction of partially shaded photovoltaic system," *Energies*, vol. 15, no. 7, pp. 1–26, Mar. 2022.
- [13] L. C. Borin, E. Mattos, C. R. D. Osorio, G. G. Koch, and V. F. Montagner, "Robust PID controllers optimized by PSO algorithm for power converters," in *Proc. IEEE 15th Brazilian Power Electron. Conf. 5th IEEE Southern Power Electron. Conf. (COBEP/SPEC)*, Dec. 2019, pp. 1–6.
- [14] M. A. Ebrahim, M. Becherif, and A. Y. Abdelaziz, "Dynamic performance enhancement for wind energy conversion system using moth-flame optimization based blade pitch controller," *Sustain. Energy Technol. Assessments*, vol. 27, pp. 206–212, Jun. 2018.
- [15] S. V. Devaraj, M. Gunasekaran, E. Sundaram, M. Venugopal, S. Chenniappan, D. J. Almakhlis, U. Subramaniam, and M. S. Bhaskar, "Robust queen bee assisted genetic algorithm (QBGA) optimized fractional order PID (FOPID) controller for not necessarily minimum phase power converters," *IEEE Access*, vol. 9, pp. 93331–93337, 2021.
- [16] A. Prakash and C. Naveen, "Combined strategy for tuning sensor-less brushless DC motor using SEPIC converter to reduce torque ripple," *ISA Trans.*, vol. 2022, pp. 1–15, Jul. 2022.
- [17] A. Wang, Z. Huang, C. Lei, Z. Chao, and E. Wu, "Parameters optimization study and analysis of PID controller in buck converter based on fuzzy particle swarm optimization algorithm," in *Proc. Int. Conf. Inf. Sci., Electron. Electr. Eng.*, Apr. 2014, pp. 1562–1566.
- [18] S.-Y. Chen, B.-C. Yang, T.-A. Pu, C.-H. Chang, and R.-C. Lin, "Active current sharing of a parallel DC–DC converters system using bat algorithm optimized two-DOF PID control," *IEEE Access*, vol. 7, pp. 84757–84769, 2019.
- [19] Z. Qi, J. Tang, J. Pei, and L. Shan, "Fractional controller design of a DC–DC converter for PEMFC," *IEEE Access*, vol. 8, pp. 120134–120144, 2020.
- [20] M. I. Mohamed, G. El-Saad, and A. M. Yousef, "Performance analysis of genetic algorithm and ant colony optimization dependent on PID controller for matrix converter," in *Proc. Int. Conf. Electron. Eng. (ICEEM)*, Jul. 2021, pp. 1–6.
- [21] K. A. Tehrani, A. Amirahmadi, S. M. R. Rafiei, G. Griva, L. Barrandon, M. Hamzaoui, I. Rasoanarivo, and F. M. Sargos, "Design of fractional order PID controller for boost converter based on multi-objective optimization," in *Proc. 14th Int. Power Electron. Motion Control Conf.*, Sep. 2010, pp. T3-179–T3-185.
- [22] S. Arun and T. Manigandan, "Design of ACO based PID controller for zeta converter using reduced order methodology," *Microprocessors Microsyst.*, vol. 81, Mar. 2021, Art. no. 103629.
- [23] C. Bhuvaneshwari and R. S. R. Babu, "Error measurement of LCC resonant converter for X-ray," *Russian J. Nondestruct. Test.*, vol. 56, no. 4, pp. 375–385, Jun. 2020.
- [24] O. Abdallah, T. O. Sweidan, M. A. Hattab, M. I. Abuashour, and M. AlMa'aitah, "Optimisation of PID controller employing PSO algorithm for interleaved buck–boost power electronic converter," *Int. J. Ind. Electron. Drives*, vol. 5, no. 1, p. 49, 2019.
- [25] I. Ahmadianfar, A. A. Heidari, A. H. Gandomi, X. Chu, and H. Chen, "RUN beyond the metaphor: An efficient optimization algorithm based on Runge Kutta method," *Expert Syst. Appl.*, vol. 181, Nov. 2021, Art. no. 115079.
- [26] L. Abualigah, D. Yousri, M. A. Elaziz, A. A. Ewees, M. A. A. Al-Qaness, and A. H. Gandomi, "Aquila optimizer: A novel meta-heuristic optimization algorithm," *Comput. Ind. Eng.*, vol. 157, Jul. 2021, Art. no. 107250.
- [27] R. Liu, T. Wang, J. Zhou, X. Hao, Y. Xu, and J. Qiu, "Improved African vulture optimization algorithm based on quasi-oppositional differential evolution operator," *IEEE Access*, vol. 10, pp. 95197–95218, 2022.
- [28] Y. Yang, H. Chen, A. A. Heidari, and A. H. Gandomi, "Hunger games search: Visions, conception, implementation, deep analysis, perspectives, and towards performance shifts," *Expert Syst. Appl.*, vol. 177, Sep. 2021, Art. no. 114864.
- [29] D. Izci, S. Ekinci, and S. Mirjalili, "Optimal PID plus second-order derivative controller design for AVR system using a modified Runge Kutta optimizer and Bode's ideal reference model," *Int. J. Dyn. Control*, vol. 2022, pp. 1–18, Oct. 2022.
- [30] H. T. Kahraman, S. Aras, and E. Gedikli, "Fitness-distance balance (FDB): A new selection method for meta-heuristic search algorithms," *Knowl.-Based Syst.*, vol. 190, Feb. 2020, Art. no. 105169.
- [31] S. Aras, E. Gedikli, and H. T. Kahraman, "A novel stochastic fractal search algorithm with fitness-distance balance for global numerical optimization," *Swarm Evol. Comput.*, vol. 61, Mar. 2021, Art. no. 100821.
- [32] U. Guvenc, S. Duman, H. T. Kahraman, S. Aras, and M. Kati, "Fitness-distance balance based adaptive guided differential evolution algorithm for security-constrained optimal power flow problem incorporating renewable energy sources," *Appl. Soft Comput.*, vol. 108, Sep. 2021, Art. no. 107421.
- [33] S. Duman, H. T. Kahraman, U. Guvenc, and S. Aras, "Development of a Lévy flight and FDB-based coyote optimization algorithm for global optimization and real-world ACOPF problems," *Soft Comput.*, vol. 25, no. 8, pp. 6577–6617, Mar. 2021.
- [34] H. Bakir, U. Guvenc, H. T. Kahraman, and S. Duman, "Improved Lévy flight distribution algorithm with FDB-based guiding mechanism for AVR system optimal design," *Comput. Ind. Eng.*, vol. 168, Jun. 2022, Art. no. 108032.
- [35] S. Duman, H. T. Kahraman, Y. Sonmez, U. Guvenc, M. Kati, and S. Aras, "A powerful meta-heuristic search algorithm for solving global optimization and real-world solar photovoltaic parameter estimation problems," *Eng. Appl. Artif. Intell.*, vol. 111, May 2022, Art. no. 104763.
- [36] E. Cengiz, C. Yilmaz, H. T. Kahraman, and C. Suicmez, "Improved Runge Kutta optimizer with fitness distance balance-based guiding mechanism for global optimization of high-dimensional problems," *Duzce Univ. J. Sci. Technol.*, vol. 9, pp. 135–149, Dec. 2021.
- [37] S. Alghamdi, H. F. Sindi, M. Rawa, A. A. Alhussainy, M. Calasan, M. Micev, Z. M. Ali, and S. H. E. Abdel Aleem, "Optimal PID controller for AVR systems using hybrid simulated annealing and gorilla troops optimization," *Fractal Fractional*, vol. 6, no. 682, pp. 1–23, Nov. 2022.
- [38] Z.-L. Gaing, "A particle swarm optimization approach for optimum design of PID controller in AVR system," *IEEE Trans. Energy Convers.*, vol. 19, no. 2, pp. 384–391, Jun. 2004.
- [39] A. Aldemir and M. S. Anwer, "Determination of optimal PID control parameters by response surface methodology," *Int. Adv. Researches Eng. J.*, vol. 2020, pp. 142–153, Aug. 2020.
- [40] D. Izci, S. Ekinci, and B. Hekimoğlu, "A novel modified Lévy flight distribution algorithm to tune proportional, integral, derivative and acceleration controller on buck converter system," *Trans. Inst. Meas. Control*, vol. 44, no. 2, pp. 393–409, Aug. 2021.
- [41] S. M. A. Altbawi, A. S. B. Mokhtar, T. A. Jumani, I. Khan, N. N. Hamadneh, and A. Khan, "Optimal design of fractional order PID controller based automatic voltage regulator system using gradient-based optimization algorithm," *J. King Saud Univ.-Eng. Sci.*, vol. 2021, pp. 1–13, Aug. 2021.
- [42] R. Pradhan, S. K. Majhi, J. K. Pradhan, and B. B. Pati, "Optimal fractional order PID controller design using ant lion optimizer," *Ain Shams Eng. J.*, vol. 11, no. 2, pp. 281–291, Jun. 2020.



EVREN ISEN was born in Bandirma, Turkey. He received the B.S., M.S., and Ph.D. degrees in electrical engineering from Yildiz Technical University, Istanbul, Turkey, in 2003, 2005, and 2011, respectively.

From 2005 to 2012, he was a Research Assistant with the Electrical Engineering Department, Yildiz Technical University. From 2012 to 2019, he was an Assistant Professor with the Electrical & Electronics Engineering Department, Kirklareli University. Since 2019, he has been an Assistant Professor with the Electrical Engineering Department, Bandirma Onyedi University. His research interests include DC/DC converters, power electronics in photovoltaic systems, and optimization techniques.